

Electronic structure and optical properties of serpentine superlattice quantum-wire arrays

Craig Pryor

Physics Department, University of California at Santa Barbara, Santa Barbara, California 93106

(Received 10 June 1991)

The subband structure and band-to-band optical matrix elements are computed for serpentine superlattice quantum-wire arrays. The subband dispersion and bandwidths are examined as a function of the curvature of the confining barriers and of the barrier height separating the wires. The optical matrix elements show a strong polarization dependence, even when the coupling between wires in the array is sufficiently strong that the states are not quasi-one-dimensional.

INTRODUCTION

The confinement of electrons and holes to quasi-one-dimensional structures holds the promise of interesting physics. One method of fabricating nanometer scale wires has been the tilted superlattice (TSL), produced by epitaxial growth on a vicinal substrate.¹ A variation on this structure has shown strong optical anisotropy, which has been interpreted as indicating two-dimensional confinement,² although the measured and calculated anisotropies are at odds with one another.³ The TSL suffers from the problem that the cross-section geometry and the coupling between wires in the array are highly sensitive to the growth rate. This makes it difficult to control the geometry and electronic properties of the resulting structure. Recently a structure was proposed that overcomes these difficulties and holds the promise of allowing the fabrication of uniform and controllable quantum-wire arrays.⁴ This structure, the serpentine superlattice (SSL), is insensitive to uncertainties in the growth rate because the rate is intentionally changed.

A cross section of the SSL wire array we will consider is shown in Fig. 1. The wells and barriers consist of GaAs and $\text{Al}_x\text{Ga}_{1-x}\text{As}$, respectively, and the barrier-well interfaces are parabolas displaced in the y direction. Confinement in the y direction is provided in the usual manner by the potential barriers. The confinement in the x direction, however, comes about because the parallel displaced parabolas produce a narrowing of the well. As one moves out along the parabola the perpendicular distance between barriers decreases, and the carriers are thus confined to the regions at the bottoms of the parabolas where the wells are widest. While the electronic structure of quantum wires has been extensively investigated theoretically,^{5,3} the structures usually considered rely on confinement by a potential barrier on all sides. The confinement in the SSL warrants another look at quantum wires.

For the purposes of calculation, the SSL will be idealized to depend on three parameters. The first is the curvature of the parabolas, which affects the confinement in the x direction. In this paper the curvature will be parametrized by q , where $y = \frac{1}{2}qx^2$ gives the contour of the barriers. Note that q is related to z_0 in Ref. 4 by

$q = 1/z_0$. The second parameter is the height of the barriers. Ideally one would like GaAs wells and AlAs barriers. Due to imperfect segregation during the growth process, however, the actual composition is $\text{Al}_x\text{Ga}_{1-x}\text{As}$ in both well and barrier, with $x_{\text{barrier}} > x_{\text{well}}$. While the total Al content averaged over wells and barriers is a well-controlled quantity, its distribution between the wells and barriers is neither ideal nor controllable.⁶ In this paper it will be assumed that the compositions within the well and barrier are each uniform and there is an abrupt interface between the well and barrier. There is evidence that the well-barrier interface is somewhat smeared,⁶ however the abrupt interface will serve as a first approximation. Finally, the properties of the SSL will depend on the period in the y direction, L_y , which is equal to the step width of the misoriented substrate.

METHOD

Energies and wave functions for the SSL were calculated in the envelope approximation assuming decoupled

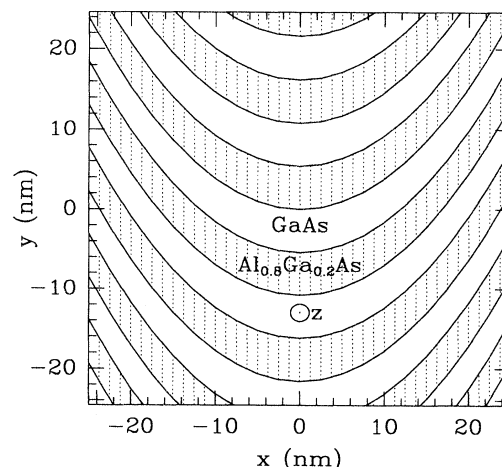


FIG. 1. Cross section of the SSL wire array considered in this paper. The barrier-well interfaces follow $y = (3.82 \times 10^{-2} \text{ nm}^{-1})x^2$, and the period in the y direction is $L_y = 10.8 \text{ nm}$. Throughout this paper the axes are shown in the figure. The z axis, which is parallel to the wires, points out of the page.

conduction and valence bands. A single period of the SSL was taken as the unit cell, in which the two-dimensional Schrödinger equation was solved numerically. In the y direction the structure is periodic, while the boundaries in the x direction were taken to be hard walls. In reality the hard walls should be barriers with finite height corresponding to the composition of the cladding layers. For the interesting cases in which the curvature of the SSL provides confinement, however, the wave function does not see the hard walls and the boundary is unimportant.

The electron Hamiltonian was taken to be

$$H = \nabla \cdot \left[\frac{-\hbar^2}{2m(\mathbf{x})} \nabla \right] + V(\mathbf{x}), \quad (1)$$

where the effective mass $m(\mathbf{x})$ and potential $V(\mathbf{x})$ depend on the local composition. For a local composition $\text{Al}_x\text{Ga}_{1-x}\text{As}$ the effective mass is

$$m = (0.0665 + 0.0835x)m_e. \quad (2)$$

The prescription used in Eq. (1) for a varying effective mass is by no means unique⁷ and Eq. (1) was chosen for its simplicity. The electron and hole effective potentials were taken to be 0.57 and 0.43 of the band offset, respectively, with the change in the gap's dependence on Al concentration given by⁸

$$\Delta E_g = 1.525x + 0.438x(1-x) \text{ eV} \quad (3)$$

at the Γ point.

The valence subbands were computed using the Luttinger Hamiltonian.⁹ The split-off $J = \frac{1}{2}$ components were ignored and only the $J = \frac{3}{2}$ components were included. The alloy composition dependence of the Luttinger parameters $\gamma_1, \gamma_2, \gamma_3$ was accounted for by linearly interpolating between the values for GaAs and AlAs, 6.85, 2.10, 2.90 and 3.25, 0.64, 1.21, respectively.¹⁰ Rather than allowing the Luttinger parameters to vary spatially, they were chosen on the basis of the alloy composition in the well. These values were used everywhere, including inside the barrier region, in which they are incorrect. Since the penetration of the wave function into the barrier is minimal, the effect of using the wrong Luttinger parameters inside the barrier is small. This approximation may be justified by noting that the inclusion of a spatially varying effective mass for the electrons led to energies differing by at most a few percent from the energies obtained using a constant mass appropriate for the well region. The holes penetrate the barriers even less due to their higher effective mass, and we therefore expect uniform Luttinger parameters to introduce errors of only a few percent.

The unusual geometry of the SSL makes analytic computations difficult. The choice of a basis set for a variational calculation is unclear, and there appears to be no change of coordinates, which simplifies the geometry. The technique used was to solve Schrödinger's equation on a lattice of points using a sparse matrix method. The derivatives in the Hamiltonian were replaced with differences on a square lattice and the resulting matrix was diagonalized using the Lanczos method.¹¹ So that

energies would be continuous functions of the curvature parameter q , the columns of the lattice were aligned with the parabolic contours. The finite differences were then computed by linear interpolation between lattice sites. Using finite differences in this manner requires less computation than a full tight-binding treatment while providing the versatility to consider any wire cross section.

The optical properties were determined by computing the band-to-band optical matrix elements, neglecting exciton effects. The envelope wave functions were computed at zone center, and from these the squares of the optical matrix elements were calculated,

$$I_\epsilon = |\langle \text{valence} | \hat{\epsilon} \cdot \nabla | \text{conduction} \rangle|^2, \quad (4)$$

where $\hat{\epsilon}$ is the unit polarization vector.

Unless otherwise stated the structure considered was that shown in Fig. 1, with a nominal Al concentration of $x = 0.8$ in the barrier and $x = 0.0$ in the well, and equal-width barriers and wells. These nominal values were chosen so that even in the worst case of no segregation ($x_{\text{barrier}} = x_{\text{well}} = 0.4$) there would still be a direct gap, making it sensible to talk about optical properties. For the nominal x values the potential barriers are 655 and 494 meV for the electrons and holes, respectively. The period in the y direction was taken to be $L_y = 10.8$ nm, corresponding to a substrate misorientation of 1.5° , and the wells and barriers were each 5.4 nm wide. The structure spanned 49.68 nm in the x direction, and the parabolas were centered in this layer. The lattice used was 20×92 , corresponding to a lattice spacing of 0.54 nm.

RESULTS

The most graphic demonstrations of the SSL are the electron wave functions shown in Fig. 2. Two wave functions, the ground and first excited states, are shown in adjacent wires for the ideal situation of GaAs wells and $\text{Al}_{0.8}\text{Ga}_{0.2}\text{As}$ barriers, and a curvature parameter of $q = 7.64 \times 10^{-2} \text{ nm}^{-1}$. The outermost contour is down by more than a factor of 10, so the wave functions appear to be well confined to the bottom of the parabolas. Note

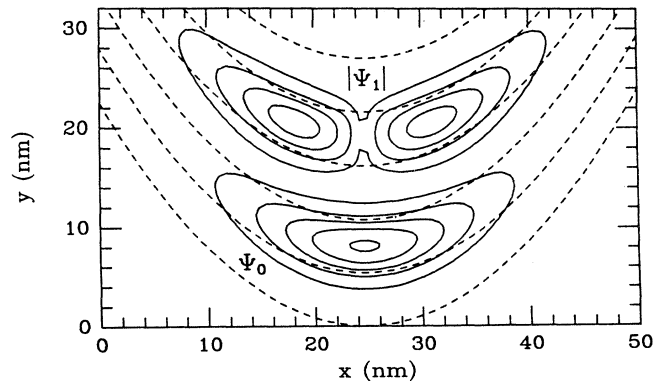


FIG. 2. Conduction-band wave functions for the ground and first excited states for ideal wires with $x_{\text{barrier}} = 0.8$ and $x_{\text{well}} = 0$. The outermost contour is 0.1 of the value at the peak.

that the first excited state extends further in the x direction, but is still confined by the SSL. For higher-lying states the wave function spreads out along the crescent, adding nodes. This is an indication of the relatively weak confinement in the x direction.

While the wave functions look wirelike, a more quantitative measure is needed. For this we examine the subband dispersion, shown in Figs. 3(a) and 3(b). Here, energies are given with respect to the conduction- and valence-band edges in the well. We see that the conduction subbands along the wire are parabolic, while in the y direction (along the wire array) the subbands are nearly flat, indicating nearly decoupled wires with a maximum subband spacing of 29 meV.

The hole subbands display much more structure, with highly nonparabolic dispersion along the wires. Also, due to the breaking of inversion symmetry at nonzero k_z the hole degeneracy is split. The valence subbands in the y direction are flatter than those for the conduction band, reflecting the fact that the higher hole mass leads to less coupling between the wires. The higher effective mass also decreases the maximum subband spacing to only 4 meV.

The effects of the geometry may be seen by examining the conduction subband energies as a function of the curvature of the parabolic potential profile. In Fig. 4 we see the energies at zone center and at $k_y = \pi/L_y$ as a function of the curvature parameter q , with the difference between these two energies giving the bandwidth. The composition is again GaAs in the wells and $\text{Al}_{0.8}\text{Ga}_{0.2}\text{As}$ in the

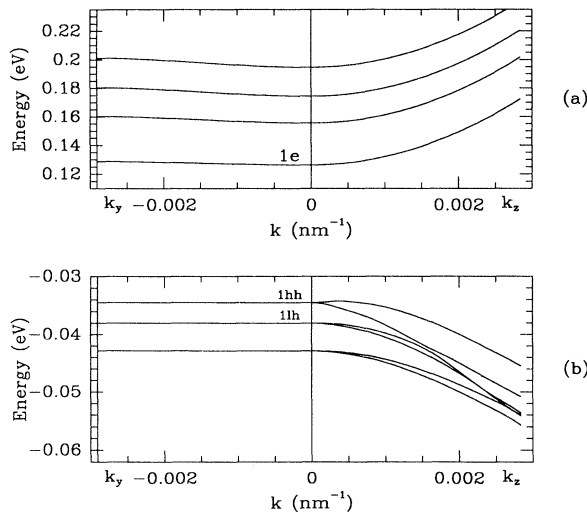


FIG. 3. (a) Conduction subband dispersion for $x_{\text{barrier}}=0.8$, $x_{\text{well}}=0$, $L_y=10.8$ nm, and $q=7.64 \times 10^{-2} \text{ nm}^{-1}$. Wave vectors are along the wires (k_z) and perpendicular to the wires in the plane of the array (k_y). Energies are with respect to the band edge in the well, and the lowest state is labeled 1e. (b) The valence subbands for the same structure. The bands are labeled as lh or hh according to the predominant component of the wave function, although the states are mixtures of heavy and light holes.

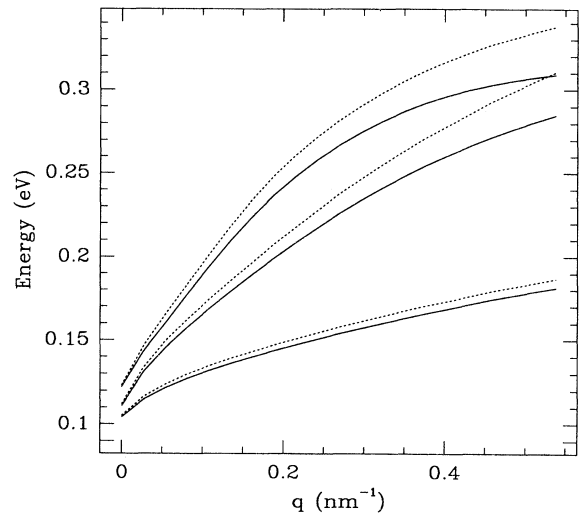


FIG. 4. Conduction-band energies as a function of the curvature parameter q with $x_{\text{barrier}}=0.8$, $x_{\text{well}}=0$, and $L_y=10.8$ nm. Solid lines indicate zone-center energies, while the dotted lines are for $k_y = \pi/L_y = 0.29 \text{ nm}^{-1}$. Note that the second and third subbands overlap for $q > 0.5 \text{ nm}^{-1}$.

barriers. For $q=0$ we have an array of wires with rectangular cross section due to the confinement from the cladding layers. As the curvature increases, the confinement in the x direction increases the confinement energy and the subband spacing. While the subband spacing is increasing, the higher confinement energy means there is more coupling through the barriers, and hence greater subband widths. Notice that for $q > 0.5 \text{ nm}^{-1}$ the second and third subband are overlapping although the lowest subband remains wirelike. This gives the largest subband spacing of approximately 100 meV, but also gives a 5-meV bandwidth for the lowest subband.

So far we have considered ideal and, given vicinal growths reported to date, somewhat unrealistic structures. As already mentioned, the most serious problem with the SSL is that both the barrier and well are $\text{Al}_x\text{Ga}_{1-x}\text{As}$, but with different (and uncontrollable) values of x . For this reason it is of interest to examine the properties of the SSL as a function of the Al distribution. In particular, poor Al segregation produces small potential barriers, leading to delocalized bands rather than confined wire states. In Figs. 5(a) and 5(b) we see the electron and hole energies at zone center at $k_y = \pi/L_y$ as a function of x in the barrier region with $x_{\text{barrier}} + x_{\text{well}} = 0.8$ held constant. The energies shown are the confinement energy above (or below) the band edges in the well. Since the gap varies with composition according to Eq. (3), transition energies would be given by the sum of the energies in Figs 5(a) and 5(b) and the gap appropriate for the well composition. By leaving out the band gap the effects of confinement are more apparent. Also, since the confinement energy depends only on the difference between the band edges in the well and barrier, the curves are applicable to any composition,

provided that the geometry is the same as that considered here.

At the far left of Fig. 5(a) we have $x_{\text{barrier}}=0.4$ and $x_{\text{well}}=0.4$, which due to the cladding layers is simply a quantum well. As x_{barrier} increases x_{well} decreases, and we begin to see two-dimensional confinement. At $x_{\text{barrier}} \approx 0.55$, corresponding to a barrier height of 416 meV, the two lowest conduction subbands become non-overlapping and the states may be said to be wirelike. For $x_{\text{barrier}} > 0.55$ the width of the lowest subband is < 10 meV, while with perfect Al segregation the bandwidth is approximately 2 meV.

The situation for the valence subbands is much better. As can be seen in Fig. 5(b), the valence subbands become nonoverlapping for $x_{\text{barrier}} > 0.45$, and with increasing segregation the bandwidths become very narrow. For $x_{\text{barrier}} > 0.5$ the bandwidth for the valence highest subband is less than 1 meV.

In the valence band the confinement introduces mixing between the heavy- and light-hole states. The degree of mixing depends on the quality of the confinement, and therefore on the curvature parameter q and the segregation. We could examine the wave functions directly, however we can make closer contact with observable quantities by examining the polarization dependence of optical matrix elements which reflect the underlying valence subband wave functions.

The polarization dependence of the band-to-band optical matrix elements is shown in Figs. 6(a)–6(c). The

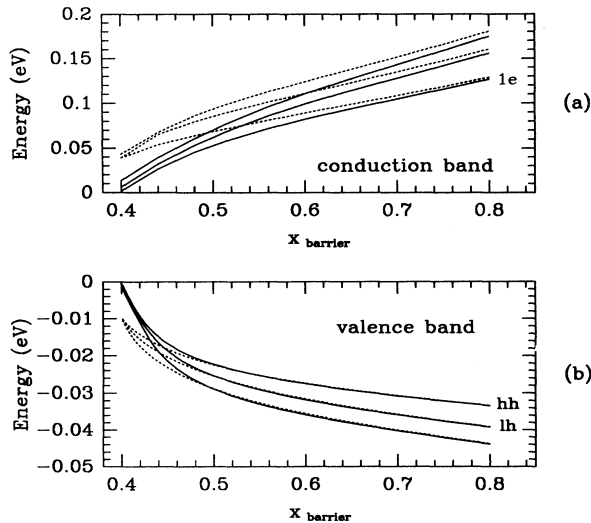


FIG. 5. (a) Conduction subband energies as a function of x_{barrier} with $x_{\text{barrier}} + x_{\text{well}} = 0.8$ and $k_z = 0$. The geometry is again that of Fig. 1 with $q = 7.64 \times 10^{-2} \text{ nm}^{-1}$. Energies are measured from the conduction-band edge in the well. Solid lines indicate zone-center energies, while the dotted lines are for $k_y = \pi/L_y = 0.29 \text{ nm}^{-1}$. (b) Valence subband energies as a function of x_{barrier} with $x_{\text{barrier}} + x_{\text{well}} = 0.8$ and $k_z = 0$. Energies are measured from the valence-band edge in the well. Solid lines indicate zone-center energies, while the dotted lines are for $k_y = \pi/L_y = 0.29 \text{ nm}^{-1}$. Note the transition from quantum-well to quantum-wire behavior takes place at a lower x_{barrier} than for the electrons.

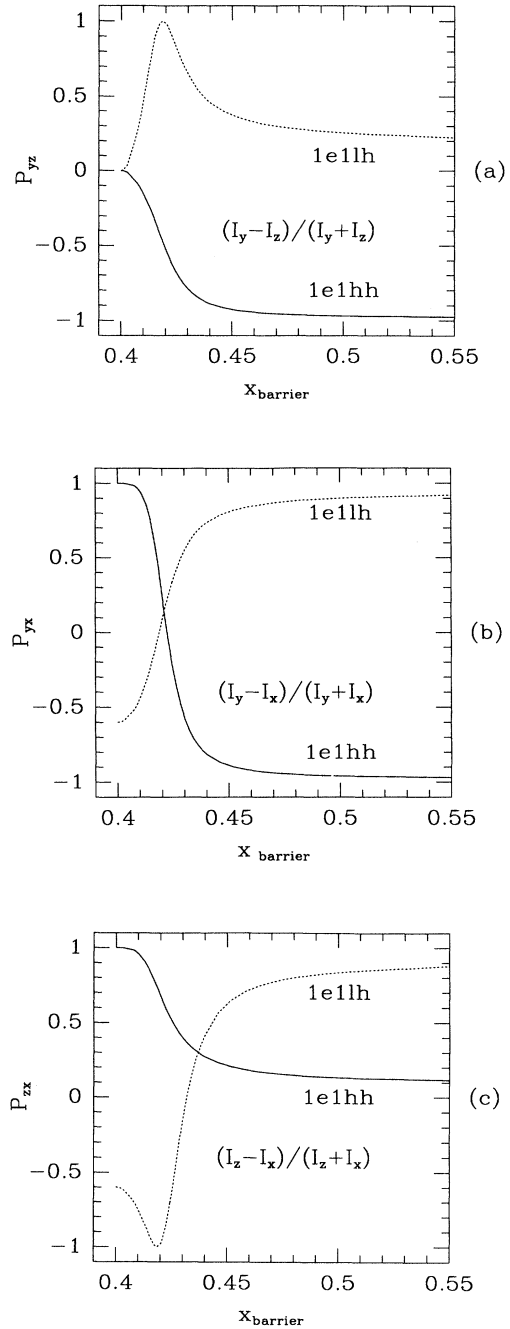


FIG. 6. (a) Polarization dependence of band-to-band optical matrix elements as a function of x_{barrier} for light emitted perpendicular to the wire array. The transitions shown are between the lowest conduction-band state, $1e$, and the two highest valence-band states, $1hh$ and $1lh$. The quantity $P_{yz} = (I_y - I_z)/(I_y + I_z)$ is plotted where I_i is the square of the matrix element for light polarized in the \hat{i} direction. (b) Polarization dependence of band-to-band optical matrix elements as a function of x for light emitted parallel to the wires. (c) Polarization dependence of band-to-band optical matrix elements as a function of x_{barrier} for light emitted perpendicular to the wires, but in the plane of the array.

quantity

$$P_{ij} = (I_i - I_j) / (I_i + I_j) \quad (5)$$

is plotted as a function of x_{barrier} , where I_i is the square of the optical matrix element for light polarized in the i direction. Again the total Al content is assumed fixed so that $x_{\text{barrier}} + x_{\text{well}} = 0.8$. The P_{ij} 's for transitions between the lowest conduction-band state and the two highest valence subband states were calculated. These two valence subband states are labeled as light and heavy hole according to the predominant component of the wave function. The highest-lying valence subband state was primarily heavy hole, while the next highest state was predominantly light hole.

Light emitted perpendicular to the wire array [Fig. 6(a)] is unpolarized for $x_{\text{barrier}} = 0.4$ since this is simply a quantum well in the plane of the SSL array. As x_{barrier} increases, the $1e1hh$ transition becomes polarized along the wires. In the limit of completely decoupled wires (large x_{barrier}) the polarization becomes very strong, with $P_{yz} \approx 0.95$. This is in agreement with calculations for single wires with rectangular cross section, for which the light from the $1e1hh$ transition is polarized along the wire.¹² The $1e1lh$ transition displays more complex behavior. From no polarization dependence P_{yz} rises to 1.0 at $x_{\text{barrier}} \approx 0.42$, but then falls with increasing barrier height, reaching the limiting value of $P_{yz} \approx 0.2$.

Light emitted in the plane of the array displays strong polarization dependence as well. For $x_{\text{barrier}} = 0.4$ we see the polarization expected of a quantum well, with $P_{yx} = P_{zx}$. Figures 6(b) and 6(c) show that with increasing x_{barrier} , P_{yx} and P_{zx} begin to differ. In the limit of decoupled wires the light emitted perpendicular to the wires has $P_{zx} \approx 0.1$ and 0.9 for $1e1hh$ and $1e1lh$, respectively. Note that for the $1e1lh$ transition P_{zx} has an extremum at $x_{\text{barrier}} \approx 0.42$, just as was seen for P_{yz} for the $1e1lh$ transition. Also note that the P_{ij} 's saturate for $x_{\text{barrier}} > 0.5$, reflecting the fact that the optical anisotropy depends on the valence subbands, which are wirelike even with poor Al segregation. Although the P_{ij} 's saturate, the anisotropy of the decoupled wires still reflects the underlying structure of the SSL. For a rectangular wire the P_{ij} 's depend on the aspect ratio,¹³ while for the SSL the detailed shape of the wire cross section will determine these quantities.

DISCUSSION

The subband dispersion and bandwidths indicate that the SSL can provide good two-dimensional confinement if the barriers are high enough. To obtain wires with subband widths less than the subband spacing requires band offsets of > 416 meV in the conduction band and > 250 meV in the valence band. We also see that the confinement of holes is significantly better than for electrons in the sense that for a given segregation narrower bandwidths are obtained for holes. It is possible to increase the subband spacing by increasing the curvature, but this is done at the expense of greater subband width.

The subband widths are small for the holes simply be-

cause the high-hole effective mass suppresses coupling of the wires through the barrier. While the coupling between wires is small, the valence subband spacing of the wires is also small because of the large effective mass. This would of course be the case for a quantum wire with potential barriers on all sides, as the confinement energy goes like $1/(mL^2)$, where L is the diameter of the wire. For the SSL, however, the situation is worse because the confinement in the x direction is due to the narrowing of the well. If we treated the narrowing of the well as an effective potential given by the confinement energy of a particle in a quantum well with infinite barriers, we would have

$$V_{\text{eff}} \propto 1/[mL^2(x)], \quad (6)$$

where $L(x)$ is the perpendicular well width in the SSL, which varies with position x . Therefore the confining potential in the x direction is weaker for larger m , and hole confinement is worse than for the electrons, even if the hole wires are less coupled to one another.

Because the confinement in the x direction for wires reported to date is weak, it controls the subband spacing. On the other hand, the bandwidth is controlled by the width and height of the barriers between wires, which are limited by the poor segregation obtained in growth on vicinal substrates. The existence of two-dimensional confinement is dictated by both the subband spacing and bandwidth. With sufficient segregation the bandwidths are much smaller than the subband spacing and wires are obtained. Wirelike hole states are obtained with poorer segregation than is needed to obtain conduction-band wires. This suggests that to observe transport anisotropies one would probably want to use p -type samples.

It is interesting that the polarization dependence is so strong. While optical anisotropy is expected in quasi-one-dimensional systems, it is interesting that the polarization is so strong for weak confinement. This is in large part due to the relatively good confinement for the hole states, upon which the anisotropy depends. However, the P_{ij} 's also show strong anisotropy for structures in which the bandwidths are large and even overlapping. This indicates that one must be cautious in interpreting optical anisotropy as a signal of two-dimensional confinement as the anisotropy may be brought about by small modulations of the hole wave function.

The strong optical anisotropy for the SSL might seem strange in light of the calculations of Citrin and Chang, who found only weak polarization for the structure of Ref. 2, in which a TSL was coupled to a quantum well (TSLQW). However, it is important to recognize the differences between that structure and the SSL, and we must examine how the wires are coupled since this determines the transition from a quantum well to decoupled wires. In the TSLQW the wires are connected by channels of GaAs, and hence the coupling between wires is of a different nature than in the SSL. A narrow GaAs channel presents an effective barrier, but with a height that depends on the channel width and effective mass according to Eq. (6). For the SSL the wires are separated by true potential barriers, for which the penetration decreases with increasing effective mass. Therefore the

TSLQW has particularly strong coupling between the wires for holes, resulting in poor optical anisotropy. This is why the calculation predicts such small polarization dependence, although it leaves unresolved the question of why the measured dependence was so strong.

ACKNOWLEDGMENTS

I wish to thank L. Sham, M. Miller, H. Weman, C. McIntyre, H. Kroemer, P. Petroff, A. Gossard, J. Merz, L. Coldren, N. Dagli, and J. Yi for helpful discussions.

-
- ¹P. M. Petroff, A. C. Gossard, and W. Weigmann, *Appl. Phys. Lett.* **45**, 620 (1984); J. M. Gaines, P. M. Petroff, H. Kroemer, R. J. Simes, R. S. Geels, and J. H. English, *J. Vac. Sci. Technol. B* **6**, 1378 (1988).
- ²M. Tsuchiya, J. M. Gaines, R. H. Yan, R. J. Simes, P. O. Holtz, L. A. Coldren, and P. M. Petroff, *Phys. Rev. Lett.* **62**, 466 (1989).
- ³D. S. Citrin and Y. C. Chang, *Appl. Phys. Lett.* **69**, 2685 (1991).
- ⁴M. S. Miller, C. E. Pryor, H. Weman, L. A. Somoska, H. Kroemer, and P. M. Petroff, *J. Cryst. Growth* **111**, 323 (1991); M. S. Miller, H. Weman, C. E. Pryor, H. Kroemer, P. M. Petroff, and J. L. Merz (unpublished).
- ⁵J. A. Brum, G. Bastard, L. L. Chang, and L. Esaki, *Superlatt. Microstruct.* **3**, 47 (1987); M. Sweeny, J. Xu, and M. Shur, *ibid.* **4**, 623 (1988).
- ⁶S. A. Chalmers, A. C. Gossard, A. L. Weisenhorn, S. A. C. Gould, B. Drake, and P. K. Hansma, *Appl. Phys. Lett.* **55**, 2491 (1989).
- ⁷Q. Zhu and H. Kroemer, *Phys. Rev. B* **27**, 3519 (1983).
- ⁸J. C. M. Henning, J. P. M. Ansens, and A. G. M. deNijs, *J. Phys. C* **17**, L915 (1984).
- ⁹J. M. Luttinger, *Phys. Rev.* **102**, 1030 (1956).
- ¹⁰*Numerical Data and Functional Relationships in Science and Technology*, edited by K. H. Hellwege, Landolt-Börnstein, New Series, Vol. III/17a (Springer, Berlin, 1982).
- ¹¹J. Cullum and R. A. Willoughby, *J. Comput. Phys.* **44**, 329 (1981).
- ¹²P. C. Sercel and K. J. Vahala, *Phys. Rev. B* **42**, 3690 (1990); *Appl. Phys. Lett.* **57**, (1990).
- ¹³C. R. McIntyre and L. Sham (unpublished).